OPEN

Correspondence and
requests for materials
should be addressed to
Z.S.L. (zslin@mail.ipc.
ac.cn)

Two novel nonlinear optical carbonates in the deep-ultraviolet region: $KBeCO_3F$ and $RbAlCO_3F_2$

Lei Kang[1,3], Zheshuai Lin[1], Jingui Qin[2] & Chuangtian Chen[1]

[1]Beijing Center for Crystal R&D, Key Lab of Functional Crystals and Laser Technology, Technical Institute of Physics and Chemistry, Chinese Academy of Sciences, Beijing 100190, PR China, [2]Department of Chemistry, Wuhan University, Wuhan 430072, PR China, [3]Graduate School of the Chinese Academy of Sciences, Beijing 100049, PR China.

With the rapid developments of the all-solid-state deep-ultraviolet (deep-UV) lasers, the good nonlinear optical (NLO) crystal applied in this spectral region is currently lacking. Here, we design two novel NLO carbonates $KBeCO_3F$ and $RbAlCO_3F_2$ from the first-principles theory implemented in the molecular engineering expert system especially for NLO crystals. Both structurally stable crystals possess very large energy band gaps and optical anisotropy, so they would become the very promising deep-UV NLO crystals alternative to KBBF. Recent experimental results on $MNCO_3F$ (M = K, Rb, Cs; N = Ca, Sr, Ba) not only confirm our calculations, but also suggest that the synthesis of the $KBeCO_3F$ and $RbAlCO_3F_2$ crystals is feasible.

Deep-ultraviolet (deep-UV, $\lambda < 200$ *nm*) nonlinear optical (NLO) crystals, as a key component of all-solid-state deep-UV lasers, have played important roles in many advanced scientific and technical areas[1–3]. Numerous attempts have been performed on the explorations of new deep-UV NLO materials with good performances[4–8], and the dominant research field has been focused on the borates[9–11]. In particular, Potassium beryllium fluoroborate ($KBe_2BO_3F_2$, KBBF) exhibits excellent NLO performance in the deep-UV region; till now KBBF is the sole NLO crystal that can practically generate the deep-UV lasers by direct SHG process[1]. However, the applications of KBBF are heavily hindered by the layering tendency in the single crystal growth processes[12]. Therefore, it is urgently demanded the emergence of new types deep-UV NLO materials.

To be a good deep-UV NLO material, the following four criterions are commonly considered[13,14]: (i) a wide UV transparency range down to the deep-UV region, corresponding to the large energy band gap and high damage threshold; (ii) a relatively large efficient second harmonic generation (SHG) coefficient ($d_{ij} \geq 0.39$ pm/V, d_{36} of KH_2PO_4); (iii) a relative large birefringence ($\Delta n \geq 0.08$) to achieve the phase matching condition in the deep-UV region; and (iv) good chemical stability and mechanical properties. According to the anionic group theory[15,16], the planar $[BO_3]^{3-}$ microscopic anionic groups have the dominant contribution to the macroscopic optical anisotropies in crystal, as in the KBBF case. Analogously, $[CO_3]^{2-}$ and $[NO_3]^-$ anionic groups are expected to be the good NLO micro-structural units as well since they have the similar planar triangle structure with the π-conjugated molecular orbitals which can produce the large birefringence and second-order susceptibility. The nitrates, however, are not considered as the NLO candidates for their hydrolysis. Thus, it is greatly desirable to explore the deep-UV NLO materials in carbonates.

The rapid developments of scientific computational resources make it possible to predict the new advanced materials directly from the first-principles theory[17–19], although search for the best candidate for a special property is still a major task[20]. In this work, aiming at the additional NLO candidates in the deep-UV region, we design two structurally stable carbonates $KBeCO_3F$ and $RbAlCO_3F_2$. The energy band gaps and the linear and nonlinear optical properties of both crystals are determined by *ab initio* calculations with high precision, which clearly demonstrate their promising applications as good optoelectronic functional materials in the deep-UV region.

Results

In order to search for the suitable deep-UV carbonates, we employed the anionic group theory combined with first-principles calculations which are implemented in the molecular engineering expert system especially for NLO crystals originated from our group[9,15]. After numerous efforts, we have theoretically discovered two carbonates, $KBeCO_3F$ and $RbAlCO_3F_2$, according to the following materials design considerations: (i) the candidates
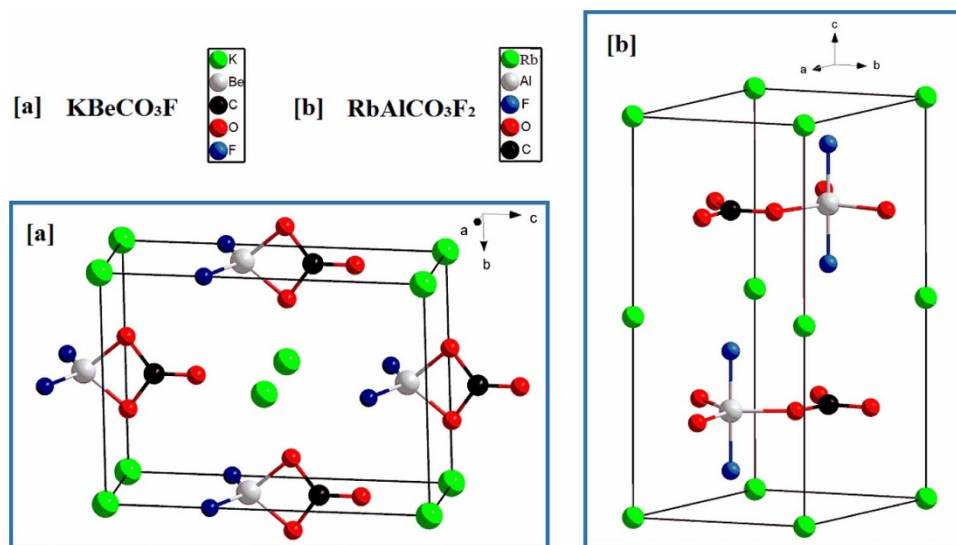
Figure 1 | Unit cell of KBeCO$_3$F (a) and RbAlCO$_3$F$_2$ (b).

are the fluoride carbonates since they can possess the larger energy band gaps compared with other carbonates[21]; (ii) the *A*-site cations are the metal cations without unclosed *d* or *f* electrons because the *d-d* or *f-f* electronic transitions have negative influences to the energy band gap. Especially the alkaline cations and the lightweight metal cations in the Group IIA and IIIA in the Periodic Table are taking into account; (iii) all [CO$_3$]$^{2-}$ anionic groups are parallel (flat-lying) with respect to the overall structural layering. This structural feature has strong optical anisotropic responses to the incident light and exhibit large optical birefringence; and (iv) the orientation of all [CO$_3$]$^{2-}$ groups is parallel to each other. This arrangement is favorable to the additive superposition of the microscopic second susceptibilities in the anionic groups, so produce large macroscopic SHG effects in crystal.

The structures of KBeCO$_3$F and RbAlCO$_3$F$_2$ are plotted in Fig. 1 (their crystallographic data see Table S1 in the Supplementary Information). In KBeCO$_3$F, the [BeO$_2$F$_2$] tetrahedra are connected with the [CO$_3$] triangles by sharing their edges, forming the zero-dimensional [BeCO$_3$F$_2$] microscopic structures isolated by the K$^+$ cations. In RbAlCO$_3$F$_2$, the [AlO$_3$F$_2$] trigonal bipyramids and [CO$_3$] triangles are alternately arranged in a trigonal pattern and connected via common O corners, generating a two-dimensional infinite [AlCO$_3$F$_2$] layer parallel to the *a*–*b* plane. The Rb$^+$ cations are located between these layers to balance charge and also hold the layers together through the coordination with O and F anions. Both structures clearly exhibit the parallel flat-lying arrangement of the [CO$_3$]$^{2-}$ groups in crystals, so they are expected to have large SHG coefficients and birefringences. More importantly, the structural stabilities of both crystals are carefully verified by the first-principles methods[18,19]. Figure 2 displays the phonon spectra and the total energy as a function of volume per atom in KBeCO$_3$F and RbAlCO$_3$F$_2$. In the phonon spectra (Figure 2(a)) none of the imaginary phonon modes is observed, and in the curves of the total energy as a function of volume per atom (Figure 2(b)) there has a single minimum in the wide range of volume modification. Both evidences clearly demonstrate that the titled crystals are kinetically stable.

The calculated linear and nonlinear optical properties for KBeCO$_3$F and RbAlCO$_3$F$_2$ are listed in Table 1, and the experimental results for KBBF are also shown as a comparison. It is clear that both KBeCO$_3$F and RbAlCO$_3$F$_2$ possess very large energy band gaps, 7.61 eV ($\sim$164 *nm*) and 8.21eV ($\sim$152 *nm*), respectively. Meanwhile, the birefringences and SHG coefficients in both

KBeCO$_3$F and RbAlCO$_3$F$_2$ crystals are larger than those in KBBF. The large birefringences ($\Delta n = 0.1297$ in KBeCO$_3$F and $\Delta n = 0.0998$ in RbAlCO$_3$F$_2$) guarantee the achievement of the SHG phase-matching condition in both crystals down to their UV absorption edge, thus their shortest phase-matching wavelengths very approach (or even exceed) the corresponding wavelength in KBBF ($\sim$161 *nm*)[12]. It should be emphasized that RbAlCO$_3$F$_2$ is optically uniaxial, which would be beneficial to its practical applications. The excellent optical properties in KBeCO$_3$F and RbAlCO$_3$F$_2$ demonstrate that both crystals are comparable to KBBF for the deep-UV SHG capabilities. Upon being obtained, these crystals would have wide applications
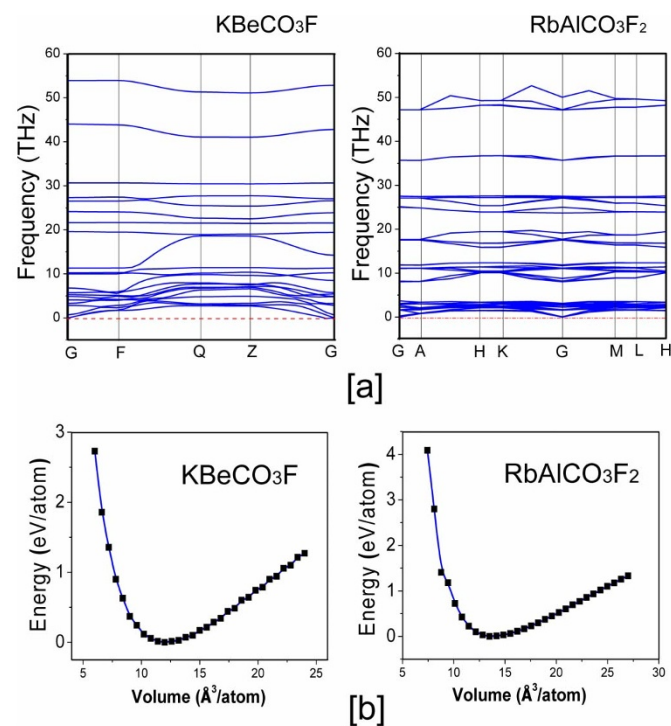

Figure 2 | Evidences of the structural stabilities in KBeCO$_3$F and RbAlCO$_3$F$_2$ from the first-principles studies. (a) The phonon spectra. (b) The total energy as a function of volume per atom. The energy minimum is set as the zero point.

Table 1 | Comparison of the linear and nonlinear optical properties in $KBeCO_3F$, $RbAlCO_3F_2$ and KBBF. E_g is the energy band gap, n is the refractive index at the wavelength $\sim 400\ nm$, Δn is the birefringence, λ_{PM} is the shortest phase-matching wavelength, and d_{ij} is the SHG coefficient. For a uniaxial crystal, $n_x = n_y = n_o$ and $n_z = n_e$

Crystal	E_g (eV)	n_x	n_y	n_z	Δn	λ_{PM} (nm)	d_{ij} (pm/V)
$KBeCO_3F$	7.61	1.5458	1.5149	1.4161	0.1297	164	$d_{21} = -0.94$; $d_{22} = 0.70$; $d_{11} = 0.26$; $d_{12} = 0.15$
$RbAlCO_3F_2$	8.21	1.4982	1.4982	1.3984	0.0998	152	$d_{16} = -d_{22} = -0.69$
KBBF[a]	8.26	1.4915	1.4915	1.4035	0.0880	161	$d_{11} = 0.47$

[a]Ref. 12.
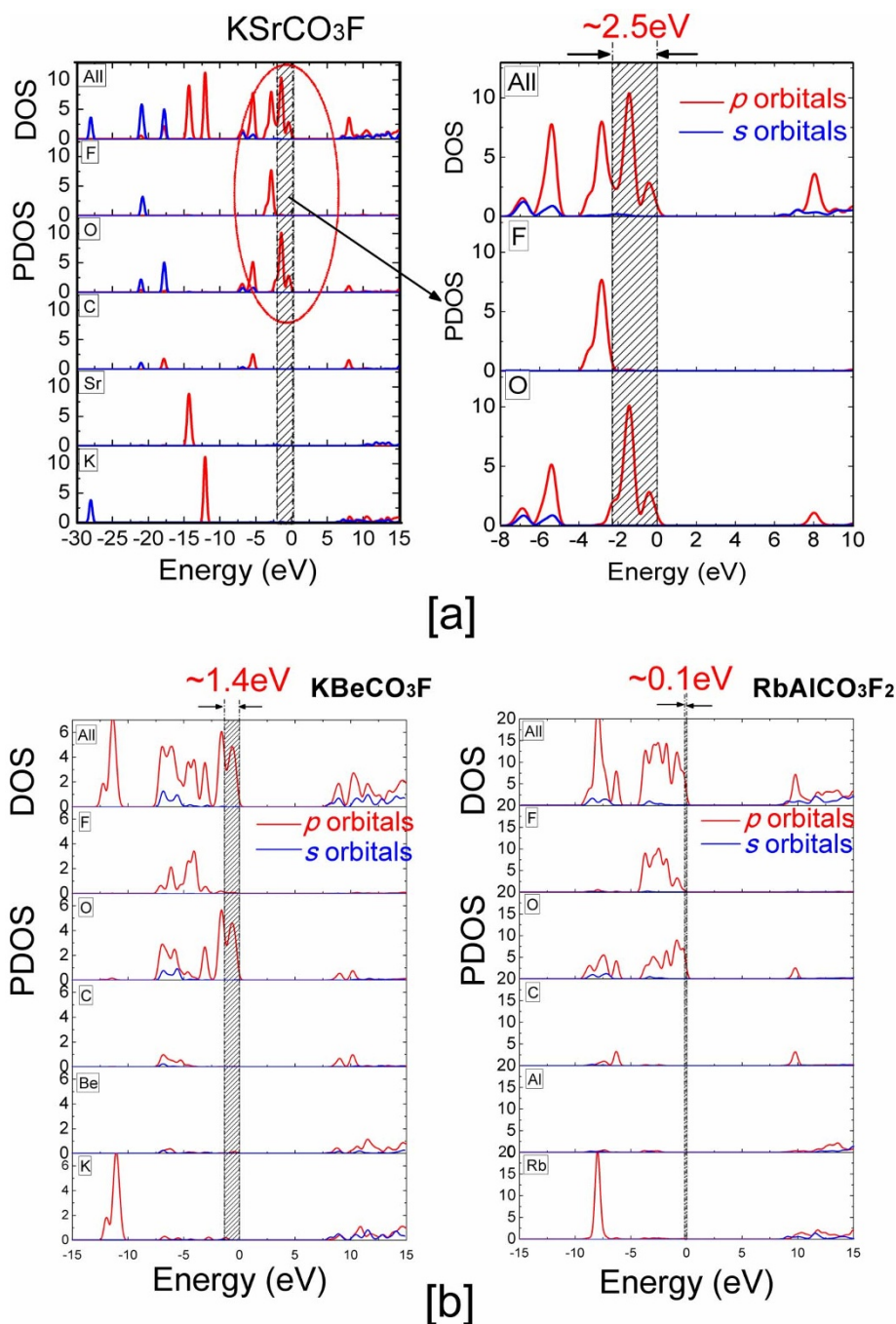
Figure 3 | (a) (left) Partial density of states (PDOS) projected on the constituent atoms in $MNCO_3F$, exemplified by the $KSrCO_3F$ crystal, (right) the PDOS zoomed-in to show the non-bonding states on oxygen atoms. (b) PDOS projected on the constituent atoms in $KBeCO_3F$ (left) and $RbAlCO_3F_2$ (right). The blue and red curves represent the s and p orbitals, respectively, and the shadow areas represent the region occupied by non-bonding states on oxygen atoms.

as the optoelectronic functional materials in the deep-UV spectral region.

Discussion

To verify the reliability of our *ab initio* calculations on the optical properties in carbonates, we also applied our calculated methods on a family of recently synthesized NLO fluoride carbonates, $MNCO_3F$ (M = K, Rb, Cs; N = Ca, Sr, Ba)[22]. The preliminary optical measures revealed that these compounds possess wide energy band gap (UV absorption edge < 200 nm) and qualitatively exhibit good capabilities for the UV harmonic generation[22]. However, due to the very small size of the samples the obtained experimental data are not enough to determine their application prospects in the deep-UV region. Our calculated energy band gaps and SHG coefficients match the available experimental results very well (see Table S2 and S3 in the Supplementary Information), which strongly prove the validity and high precision of the first-principles studies on the UV NLO carbonate crystals. Since the $MNCO_3F$ series possess strong NLO effect and large birefringence, we predict that they are suitable to be good NLO crystals and excellent birefringent materials in the UV region. Nevertheless, these carbonates cannot be applied in the deep-UV region due to their relatively small energy band gaps ($E_g \sim$ 6.3 eV).

The detailed electronic structure analysis show that the small energy gaps in $MNCO_3F$ are mainly due to the O $2p$ non-bonding states exclusively occupied at the valence band maximum, which have negligible small overlap with other electronic states and directly determine the energy band gap[23] (see Figure S1 in the Supplementary Information). The energy spanning of these non-bonding states is as large as about 2.5 eV, and their complete elimination can significantly increase the energy band gap of crystals to more than 8.3 eV (UV absorption edge < 150 nm). Compared $MNCO_3F$ with our proposed crystals, the substitution of Ca, Sr or Ba atoms with the lightweight metal cations in the Group IIA or IIIA, Be or Al, can effectively remove the non-bonding orbitals in carbonates, analogous to the borate cases such as beryllium in KBBF[24,25] and aluminum in $BaAlBO_3F$ (BABF)[26–28]. Indeed, Figure 3 clearly shows that the energy spanning of the non-bonding regions in $KBeCO_3F$ and $RbAlCO_3F_2$ reduces about 1.1 eV and 2.3 eV, respectively, compared with that in $MNCO_3F$, exemplified by $KSrCO_3F$. Therefore, the UV absorption edge of both $KBeCO_3F$ and $RbAlCO_3F_2$ are significantly blue-shifted. In addition, the similarity of the micro-structural features in the $MNCO_3F$ series and our proposed crystals suggests that it is feasible to synthesize $KBeCO_3F$ and $RbAlCO_3F_2$ in experiments.

We surveyed throughout Inorganic Crystal Structure Database (ICSD)[29], and found that only 14 fluoride carbonates whose energy band gaps may be large enough to transmit the UV radiation have been discovered and synthesized in experiments (see Table S4 in the Supplementary Information), in which seven are noncentrosymmetric and satisfy the SHG requirement. The very few report on UV NLO carbonates actually implies that the researches on this type of optoelectronic functional materials have been long-termly neglected and the broad developing space is available. We believe that our work would have great implications on the search and design of new NLO crystals in the deep-UV spectral region with the great help of advanced synthesis and single-crystal growth approaches.

Methods

First-principles computational methods and geometry optimizations. The first-principles calculations are performed by the plane-wave pseudopotential method[30] implemented in the CASTEP package[31] based on the density functional theory (DFT)[32]. The ion-electron interactions are modeled by the optimized normal-conserving pseudopotentials for all elements[33–35]. The kinetic energy cutoffs of 900 eV and Monkhorst-Pack k-point meshes[36] with the spanning of less than 0.03/Å^3 in the Brillouin zone are chosen. The supercell volume and the atomic positions for $KBeCO_3F$ and $RbAlCO_3F_2$ are fully optimized using the quasi-Newton method[37]. The convergence thresholds between optimization cycles for energy change, maximum

force, maximum stress, and maximum displacement are set as 10^{-5} eV/atom, 0.03 eV/Å, 0.05 GPa, and 0.001 Å, respectively. The above computational set ups are sufficiently accurate for present purposes[38].

Calculated methods for structural stability. To verify the structural stability, phonon spectra calculations on $KBeCO_3F$ and $RbAlCO_3F_2$ are performed. The positive eigenvalues for all phonon modes is the most important evidence for the structural stability in crystal. The structural stability can also be demonstrated by the total energy as a function of volume per atom. If there has only a single minimum in the wide range of volume modification, the studied geometrical structure would be stable. The studied methods on structural stability were also adopted by Yao[18] and Sheng[19].

Calculated methods for optical properties. When determining the linear optical properties the imaginary part of the dielectric function ε_2 is calculated[39], and then its real part is determined by Kramers-Kronig transform, from which the refractive indices (and the birefringence) are obtained. Moreover, the second-order susceptibility $\chi^{(2)}$, i.e., the SHG coefficient d_{ij}, is calculated by the following formula developed by our group[40]:

$$\chi^{\alpha\beta\gamma} = \chi^{\alpha\beta\gamma}(VE) + \chi^{\alpha\beta\gamma}(VH) + \chi^{\alpha\beta\gamma}(\text{two bands}),$$

where $\chi^{\alpha\beta\gamma}(VE)$, $\chi^{\alpha\beta\gamma}(VH)$ and $\chi^{\alpha\beta\gamma}(\text{two bands})$ denote the contributions from virtual-electron processes, virtual-hole processes and two-band processes, respectively. The formulae for calculating $\chi^{\alpha\beta\gamma}(VE)$, $\chi^{\alpha\beta\gamma}(VH)$ and $\chi^{\alpha\beta\gamma}(\text{two bands})$ are given as follows[40]:

$$\chi^{\alpha\beta\gamma}(VH) = \frac{e^3}{2\hbar^2 m^3} \times \sum_{vv'c} \int \frac{d^3k}{4\pi^3} P(\alpha\beta\gamma) \text{Im}[p_{vv'}^\alpha p_{v'c}^\beta p_{cv}^\gamma] \left(\frac{1}{\omega_{cv}^3 \omega_{v'c}^2} + \frac{2}{\omega_{vc}^4 \omega_{cv'}} \right)$$

$$\chi^{\alpha\beta\gamma}(VE) = \frac{e^3}{2\hbar^2 m^3} \times \sum_{vcc'} \int \frac{d^3k}{4\pi^3} P(\alpha\beta\gamma) \text{Im}[p_{vc}^\alpha p_{cc'}^\beta p_{c'v}^\gamma] \left(\frac{1}{\omega_{cv}^3 \omega_{vc'}^2} + \frac{2}{\omega_{vc}^4 \omega_{c'v}} \right)$$

$$\chi^{\alpha\beta\gamma}(\text{two bands}) = \frac{e^3}{\hbar^2 m^3} \times \sum_{vc} \int \frac{d^3k}{4\pi^3} P(\alpha\beta\gamma) \frac{\text{Im}[p_{vc}^\alpha p_{cv}^\beta (p_{vv}^\gamma - p_{cc}^\gamma]}{\omega_{vc}^5}$$

Here, α, β and γ are Cartesian components, v and v' denote valence bands, and c and c' denote conduction bands. $P(\alpha\beta\gamma)$ denotes full permutation and explicitly shows the Kleinman symmetry of the SHG coefficients. The band energy difference and momentum matrix elements are denotes as $\hbar\omega_{ij}$ and p_{ij}^α, respectively, and they are all implicitly k dependent.

It is well acknowledged that the DFT calculations with the exchange-correlation (XC) functional of generalized gradient approximation (GGA)[41] always underestimate the energy band gap of crystals. For calculating the optical coefficients, a scissors operator[42,43] is usually introduced to shift up all the conduction bands to agree with the measured band gap, which is not "purely" *ab initio*. Recently, we have examined several XC functionals beyond GGA on the determination of energy band gaps and optical properties in UV NLO crystals[44]. It was found that the hybrid functionals such PBE0[45], P3LYP[46] and sX-LDA[47] can predict the UV absorption edge very well, but the calculated electronic band structures and optical properties are not well reproduced compared to the scissors-corrected GGA method[44]. Indeed our calculations show that in the $MNCO_3F$ crystals the GGA energy band gaps are in large discrepancy to the experimental results (absolute error excesses 2.4 eV), while the PBE0 values are in good consistency with the measurements (see Table S2 in the Supplementary Information). Therefore, in this work the difference between PBE0 and GGA energy band gaps is set as the scissors operator, which is then used to determine the optical properties by GGA. The further tests have also revealed that the $\chi^{(2)}$ values is insensitive to the modification (e.g. $\sim \pm 0.5$ eV) of the scissors operator because of the very large band gap (>6 eV) in the studied carbonates. Therefore, this computational procedure ensures that our first-principles studies are self-consistent without adjusting any parameter from experiments.

1. Cyranoski, D. China's crystal cache. *Nature* **457**, 953–955 (2009).
2. Xu, Y. M. *et al.* Observation of a ubiquitous three-dimensional superconducting gap function in optimally doped $Ba_{0.6}K_{0.4}Fe_2As_2$. *Nature Physics* **7**, 198–202 (2011).
3. Mu, R. *et al.* Visualizing Chemical Reactions Confined under Graphene. *Angew. Chem. Int. Ed.* **51**, 4856–4859 (2012).
4. Wang, S., Ye, N., Li, W. & Zhao, D. Alkaline Beryllium Borate $NaBeB_3O_6$ and $ABe_2B_3O_7$ (A = K, Rb) as UV Nonlinear Optical Crystals. *J. Am. Chem. Soc.* **132**, 8779–8786 (2010).
5. Wang, S. & Ye, N. $Na_2CsBe_6B_5O_{15}$: An Alkaline Beryllium Borate as a Deep-UV Nonlinear Optical Crystal. *J. Am. Chem. Soc.* **133**, 11458–11461 (2011).
6. Huang, H. *et al.* $NaSr_3Be_3B_3O_9F_4$: A Promising Deep-Ultraviolet Nonlinear Optical Material Resulting from the Cooperative Alignment of the $Be_3B_3O_{12}F_{10}^-$ Anionic Group. *Angew. Chem. Int. Ed.* **50**, 9141–9144 (2011).
7. Yang, Y. *et al.* A New Lithium Rubidium Borate $Li_6Rb_5B_{11}O_{22}$ with Isolated $B_{11}O_{22}$ Building Blocks. *Cryst. Growth Des.* **11**, 3912–3916 (2011).
8. McMillen, C. D., Stritzinger, J. T. & Kolis, J. W. Two Novel Acentric Borate Fluorides: $M_3B_6O_{11}F_2$ (M = Sr, Ba). *Inorg. Chem.* **51**, 3953–3955 (2012).
9. Becker, P. Borate materials in nonlinear optics. *Adv. Mater.* **10**, 979–992 (1998).

10. Keszler, D. A. Synthesis, crystal chemistry, and optical properties of metal berates. *Curr. Opin. Solid State Mater. Sci.* **4**, 155–162 (1999).

11. Ghotbi, M. *et al.* Efficient third harmonic generation of microjoule picosecond pulses at 355 nm in BiB_3O_6. *Appl. Phys. Lett.* **89**, 173124 (2006).

12. Chen, C. T., Wang, G. L., Wang, X. Y. & Xu, Z. Y. Deep-UV nonlinear optical crystal $KBe_2BO_3F_2$---discovery, growth, optical properties and applications. *Appl. Phys. B* **97**, 9–25 (2009).

13. Chen, C. T. *et al.* Computer-assisted search for nonlinear optical crystals. *Adv. Mater.* **11**, 1071–1078 (1999).

14. Xia, Y. N., Chen, C. T., Tang, D. Y. & Wu, B. C. New nonlinear-optical crystals for UV and VUV harmonic-generation. *Adv. Mater.* **7**, 79–81 (1995).

15. Chen, C. T. *et al. Nonlinear optical borate crystals.* (Wiley-VCH, Germany, 2012).

16. Chen, C. T., Lin, Z. S. & Wang, Z. Z. The development of new borate-based UV nonlinear optical crystals. *Appl. Phys. B* **80**, 1–25 (2005).

17. Zhang, H. *et al.* Topological insulators in Bi_2Se_3, Bi_2Te_3 and Sb_2Te_3 with a single Dirac cone on the surface. *Nature Physics* **5**, 438–442 (2009).

18. Yao, Y. *et al.* Comment on "New Metallic Carbon Crystal". *Phys. Rev. Lett.* **102**, 229601 (2009).

19. Sheng, X.-L., Yan, Q.-B., Ye, F., Zheng, Q.-R. & Su, G. T-carbon: a novel carbon allotrope. *Phys. Rev. Lett.* **106**, 155703 (2011).

20. Katritzky, A. R. *et al.* Quantitative Correlation of Physical and Chemical Properties with Chemical Structure: Utility for Prediction. *Chem. Rev.* **110**, 5714–5789 (2010).

21. Grice, J. D., Maisonneuve, V. & Leblanc, M. Natural and synthetic fluoride carbonates. *Chem. Rev.* **107**, 114–132 (2007).

22. Zou, G. H., Ye, N., Huang, L. & Lin, X. S. Alkaline-Alkaline Earth Fluoride Carbonate Crystals $ABCO_3F$ (A = K, Rb, Cs; B = Ca, Sr, Ba) as Nonlinear Optical Materials. *J. Am. Chem. Soc.* **133**, 20001–20007 (2011).

23. He, R., Lin, Z. S., Zheng, T., Huang, H. & Chen, C. T. Energy band gap engineering in borate ultraviolet nonlinear optical crystals: ab initio studies. *J. Phys: Condens. Matter* **24**, 145503 (2012).

24. Lin, Z. H., Wang, Z. Z., Chen, C. T., Chen, S. K. & Lee, M. H. Mechanism for linear and nonlinear optical effects in $KBe_2BO_3F_2$ (KBBF) crystal. *Chem. Phys. Lett.* **367**, 523–527 (2003).

25. Kang, L. *et al.* Ab initio studies on the optical effects in the deep ultraviolet nonlinear optical crystals of the $KBe_2BO_3F_2$ family. *J. Phys: Condens. Matter* **24**, 335503 (2012).

26. Hu, Z. G., Yoshimura, M., Mori, Y. & Sasaki, T. Growth of a new nonlinear optical crystal-$BaAlBO_3F_2$. *J. Cryst. Growth* **260**, 287–290 (2004).

27. Yue, Y. C. *et al.* Growth and nonlinear optical properties of $BaAlBO_3F_2$ crystal. *J. Opt. Soc. Am. B* **28**, 861–866 (2011).

28. Huang, H., Lin, Z. S., Bai, L., Hu, Z. G. & Chen, C. T. Ab initio calculations on the borate nonlinear optical crystal $BaAlBO_3F_2$. *J. Appl. Phys.* **106**, 103107 (2009).

29. ICSD, 2012-1, Version 1.8.2, by Fachinformatiionszentrum Karlsruhe, Germany.

30. Payne, M. C., Teter, M. P., Allan, D. C., Arias, T. A. & Joannopoulos, J. D. Iterative minimization techniques for abinitio total-energy calculations - molecular-dynamics and conjugate gradients. *Rev. Mod. Phys.* **64**, 1045–1097 (1992).

31. Clark, S. J. *et al.* First principles methods using CASTEP. *Z. Kristall.* **220**, 567–570 (2005).

32. Kohn, W. & Sham, L. J. Self-consistent equations including exchange and correlation effects. *Phys. Rev.* **140**, 1133 (1965).

33. Rappe, A. M., Rabe, K. M., Kaxiras, E. & Joannopoulos, J. D. Optimized pseudopotentials. *Phys. Rev. B* **41**, 1227–1230 (1990).

34. Lin, J. S., Qteish, A., Payne, M. C. & Heine, V. Optimized and transferable nonlocal separable ab initio pseudopotentials. *Phys. Rev. B* **47**, 4174–4180 (1993).

35. Kleinman, L. & Bylander, D. M. Efficacious form for model pseudopotentials. *Phys. Rev. Lett.* **48**, 1425–1428 (1982).

36. Monkhorst, H. J. & Pack, J. D. Special points for brillouin-zone integrations. *Phys. Rev. B* **13**, 5188–5192 (1976).

37. Pfrommer, B. G., Cote, M., Louie, S. G. & Cohen, M. L. Relaxation of crystals with the quasi-Newton method. *J. Comput. Phys.* **131**, 233–240 (1997).

38. Plckard Chris, J. & Needs, R. J. Ab initio random structure searching. *J. Phys.: Condens. Matter* **23**, 053201 (2011).

39. Palik, E. D. Handbook of Optical Constants of Solids. Orlando: Academic Press: New York (1985).

40. Lin, J., Lee, M. H., Liu, Z. P., Chen, C. T. & Pickard, C. J. Mechanism for linear and nonlinear optical effects in beta-BaB_2O_4 crystals. *Phys. Rev. B* **60**, 13380–13389 (1999).

41. Perdew, J. P. & Wang, Y. Accurate and simple analytic representation of the electron-gas correlation-energy. *Phys. Rev. B* **45**, 13244–13249 (1992).

42. Godby, R. W., Schluter, M. & Sham, L. J. Self-energy operators and exchange-correlation potentials in semiconductors. *Phys. Rev. B* **37**, 10159–10175 (1988).

43. Wang, C. S. & Klein, B. M. 1st-principles electronic-structure of Si, Ge, GaP, GaAs, ZnS, and ZnSe.2. Optical-properites. *Phys. Rev. B* **24**, 3417–3429 (1981).

44. Lin, Z. S. *et al.* Strategy for the optical property studies in ultraviolet nonlinear optical crystals from density functional theory. *Comput. Mater. Sci.* **60**, 99–104 (2012).

45. Adamo, C. & Barone, V. Toward reliable density functional methods without adjustable parameters: The PBE0 model. *J. Chem. Phys.* **110**, 6158–6170 (1999).

46. Becke, A. D. Density-functional thermochemistry.3. The role of exact exchange. *J. Chem. Phys.* **98**, 5648–5652 (1993).

47. Seidl, A., Gorling, A., Vogl, P., Majewski, J. A. & Levy, M. Generalized Kohn-Sham schemes and the band-gap problem. *Phys. Rev. B* **53**, 3764–3774 (1996).

Acknowledgements

Author contributions

L.K. performed the first-principles studies and prepared the data. Z.S.L. supervised the studies and wrote the manuscript. J.G.Q. and C.T.C. discussed results.

Additional information

Supplementary information accompanies this paper at http://www.nature.com/scientificreports

Competing financial interests: The authors declare no competing financial interests.

How to cite this article: Kang, L., Lin, Z.S., Qin, J.G. & Chen, C.T. Two novel nonlinear optical carbonates in the deep-ultraviolet region: $KBeCO_3F$ and $RbAlCO_3F_2$. *Sci. Rep.* **3**, 1366; DOI:10.1038/srep01366 (2013).